TinA enables kinesin-14/KlpA to exhibit processive minus-end-directed motility

Akasit Visootsat[1,*], Andrew R. Popchock[2,*], Yuan Gao[1], and Weihong Qiu[1,2]

[1]Department of Physics, Oregon State University, Corvallis, Oregon 97331, USA.

[2]Department of Biochemistry and Biophysics, Oregon State University, Corvallis, Oregon 97331, USA.

*These authors contributed equally to this work.

Correspondence: Weihong.Qiu@oregonstate.edu (WQ).

ABSTRACT

Kinesin-14 motors contribute to spindle assembly by localizing to spindle poles and anchoring the minus ends of spindle microtubules. Unlike other kinesin-14 motors, KlpA uniquely exhibits plus-end-directed motility on single microtubules as individual homodimers. However, the mechanism by which KlpA achieves minus-end-directed motility on single microtubules remains elusive. Here, we report that TinA, a highly conserved microtubule-anchoring protein, serves as an activator of KlpA for minus-end-directed motility. TinA directly interacts with KlpA to form minus-end-directed complexes that exhibit continuous movement on microtubules with two distinct velocity modes. The assembly of KlpA-TinA complexes depends on TinA binding to the central stalk of KlpA. Furthermore, TinA is a microtubule-binding protein, with its C-terminal region playing a critical role in microtubule interaction. Deletion of the C-terminus of TinA markedly reduces its microtubule-binding ability and severely impairs the formation of KlpA-TinA complexes. Nonetheless, KlpA-TinA complexes formed without the C-terminus of TinA still exhibit minus-end-directed motility, albeit with a single velocity mode. Collectively, these findings provide critical mechanistic insights into how TinA modulates KlpA, enabling the kinesin-14 motor to achieve minus-end-directed motility.

53 **INTRODUCTION**

54 The mitotic spindle is a bipolar, microtubule-based structure that eukaryotic cells assemble during
55 mitosis to ensure the accurate segregation of duplicated chromosomes between daughter cells[1].
56 Microtubules are asymmetric cylindrical polymers of α/β-tubulin heterodimers with two distinct
57 ends: a highly dynamic plus end capped with β-tubulin and a less dynamic minus end capped
58 with α-tubulin[2]. The assembly of a bipolar spindle relies on the coordinated activities of kinesins[3,4],
59 motor proteins that convert chemical energy from ATP hydrolysis into forces or movements along
60 microtubules[5]. Errors in spindle assembly can result in daughter cells with abnormal chromosome
61 numbers, a hallmark of cancer[6] .

62 All kinesins contain at least one motor domain that hydrolyzes ATP and binds to
63 microtubules. Based on the sequence similarity of the motor domains, kinesins are classified into
64 14 subfamilies (kinesin-1 through kinesin-14) and an orphan group[7]. Kinesin-14s are commonly
65 homodimers consisting of an N-terminal microtubule-binding tail, a central coiled-coil stalk, a neck,
66 and two identical C-terminal motor domains[8] . Examples of homodimeric kinesin-14s include
67 HSET from *Homo sapiens*[9], Ncd from *Drosophila melanogaster*[10,11], Pkl1 from
68 *Schizosaccharomyces pombe*[12], and KlpA from *Aspergillus nidulans*[13]. Kinesin-14 motors
69 contribute to spindle assembly by using minus-end-directed motility to localize at spindle poles,
70 anchoring the minus ends of spindle microtubules[8]. Unlike all other kinesin-14 motors studied to
71 date[10,11,14–18], which either exhibit minus-end-directed motility or diffuse without directional
72 preference, KlpA uniquely displays plus-end-directed motility on single microtubules as individual
73 homodimers[19]. However, it remains unclear how KlpA achieves minus-end-directed motility for
74 localizing to the spindle poles to contribute to spindle assembly. In *S. pombe,* localization of Pkl1
75 to spindle poles depends on Msd1 and Wdr8[20], suggesting that KlpA might use a similar
76 mechanism to localize the spindle poles. Notably, Msd1 and Wdr8 are conserved in many
77 eukaryotic organisms[21], with homologs in *A. nidulans* identified as TinA and AnWdr8,
78 respectively[22].

79 In this study, we focused on characterizing the effect of TinA on the motility of KlpA. We
80 found that TinA binds to the central stalk of KlpA, forming KlpA-TinA complexes that exhibit
81 continuous minus-end-directed motility on the microtubules with both fast and slow velocities. We
82 further revealed that the C-terminus of TinA acts as a microtubule-binding tether to not only induce
83 the complexes to move with the slower velocity mode but also play an essential role in the
84 formation of the KlpA-TinA complexes. To our knowledge, TinA is the first protein shown to
85 reverse kinesin directionality through direct interaction. These findings significantly expand our
86 understanding of kinesin regulation by binding partners. Overall, our findings provided critical
87 mechanistic insights into the regulation of KlpA by TinA that enables long-distance minus-end-
88 directed motility on the microtubules.

89 **RESULTS**

90 **TinA and KlpA interact to form minus-end-directed complexes.** We set out to determine
91 whether TinA can directly interact with KlpA to affect its motility on the microtubules. To address
92 this, we first engineered fluorescently labeled KlpA and TinA (GFP-KlpA and TinA-mCherry, Fig.
93 1a), and then performed an *in vitro* total internal reflection fluorescence (TIRF) microscopy assay
94 to examine the motility of GFP-KlpA on surface-immobilized polarity-marked microtubules, both
95 in the absence and presence of TinA-mCherry (Fig. 1b). In the control motility experiments
96 containing 2.5 nM GFP-KlpA without TinA-mCherry, all but a few GFP-KlpA particles exhibited
97 plus-end-directed motility on the microtubules (Fig. 1c; Supplementary Movie 1), similar to
98 previous observations[19]. The minus-end-directed GFP-KlpA particles (white arrowhead, Fig. 1c)
99 were aggregates rather than individual homodimers, as they were much brighter than the ones
100 moving toward the microtubule plus ends. In contrast, in the motility experiments containing 2.5
101 nM GFP-KlpA and 80 nM TinA-mCherry, GFP-KlpA molecules completely lost their directional
102 preference for the microtubule plus ends and instead moved continuously toward the minus ends
103 (Fig. 1d, left panel; Supplementary Movie 2). Notably, while TinA-mCherry lacked the ability to
104 autonomously generate directional motility on the microtubules (data not shown), it became motile

105 in the presence of GFP-KlpA and co-translocated with GFP-KlpA toward the microtubule minus
106 ends (Fig. 1d, middle and right panels). Thus, TinA directly interacts with KlpA to form minus-end-
107 directed KlpA-TinA complexes.

108 We observed that minus-end-directed KlpA-TinA complexes appeared to move with two
109 different velocities (Fig. 1d, right panel, blue and white arrowheads). To verify this, we performed
110 additional motility experiments with 2.5 nM GFP-KlpA and 4 nM TinA-mCherry, which allowed us
111 to distinguish individual minus-end-directed complexes and measure their velocities (Fig. 1e;
112 Supplementary Movie 3). Quantitative kymograph analysis confirmed that the velocity distribution
113 of KlpA-TinA complexes was indeed bimodal, with the two modes corresponding to V_{slow} = 69 ±
114 17 nm/s and V_{fast} = 246 ± 74 nm/s (mean ± s.d., n = 287, Fig. 1f).

115 **TinA binds to the central stalk of KlpA.** As an initial step toward understanding how the binding
116 of TinA causes KlpA to reverse its direction of motion, we sought to determine where TinA binds
117 on KlpA. We had previously found that KlpA becomes a minus-end-directed motor when its N-
118 terminal nonmotor domain and C-terminal motor domains bind to two different microtubules[19] or
119 its central stalk is remodeled with the insertion of a flexible polypeptide[23]. These findings led us
120 to hypothesize that TinA binds to the nonmotor region of KlpA. To test this hypothesis, we
121 engineered GFP-KlpAΔN^T (Supplementary Fig. 1a) — a GCN4 leucine zipper-driven KlpA
122 tetramer containing an N-terminal GFP and the C-terminal amino acids (a.a.) 398-770 of KlpA —
123 and used TIRF microscopy to examine its motility both in the absence and presence of TinA-
124 mCherry. The results showed that GFP-KlpAΔN^T ([GFP-KlpAΔN^T] = 2.5 nM) exhibited almost
125 identical minus-end-directed motility on the microtubules both in the absence of TinA-mCherry
126 (Supplementary Fig. 1b; Supplementary Movie 4) and in its presence ([TinA-mCherry] = 80 nM;
127 Supplementary Fig. 1c; Supplementary Movie 5). In the latter experiments, no TinA-mCherry was
128 observed to co-translocate with GFP-KlpAΔN^T on the microtubules (Supplementary Fig. 1c,

129 middle and right panels). Collectively, these results suggest that the N-terminus of KlpA (a.a. 1-
130 397) is necessary for the interaction between TinA and KlpA.

131 We next wanted to determine whether the N-terminal region of KlpA (a.a. 1-397) is
132 sufficient for the interaction with TinA. To address this, we engineered GFP-KlpA*Ncd-#1 (Fig. 2a)
133 — a chimera containing an N-terminal GFP followed by the N-terminal a.a. 1-397 of KlpA and the
134 C-terminal motor domains of Ncd (a.a. 305-700) — and examined its motility on the microtubules
135 both in the absence and presence of TinA-mCherry. The motor domains of Ncd were chosen for
136 making GFP-KlpA*Ncd-#1, because GFP-Ncd lacked the ability to interact with TinA-mCherry to
137 form minus-end-directed complexes in the control motility experiments (Supplementary Fig. 1d,e;
138 Supplementary Movie 6, 7). In the motility experiments with 2.5 nM GFP-KlpA*Ncd-#1 in the
139 absence of TinA-mCherry, GFP-KlpA*Ncd-#1 exhibited diffusive motion on the microtubules with
140 no directional preference for either end (Fig. 2b; Supplementary Movie 8). In contrast, in motility
141 experiments with 2.5 nM GFP-KlpA*Ncd-#1 and 80 nM TinA-mCherry, GFP-KlpA*Ncd-#1 gained
142 the ability to generate directional motility on the microtubules and co-translocated with TinA-
143 mCherry continuously toward the minus ends (Fig. 2c; Supplementary Movie 9), similar to what
144 we observed in the motility experiments with 2.5 nM GFP-KlpA and 80 nM TinA-mCherry (Fig.
145 1d). Thus, the N-terminal region of KlpA (a.a. 1-397) is sufficient for the interaction between TinA
146 and KlpA.

147 To further narrow down the region on KlpA involved in the interaction with TinA, we created
148 GFP-KlpA*Ncd-#2 (Fig. 2a), a chimera derived from GFP-KlpA*Ncd-#1 by replacing the region
149 corresponding to the tail of KlpA (a.a. 1-100) with that of Ncd (a.a. 1-117). We found that in the
150 absence of TinA-mCherry, GFP-KlpA*Ncd-#2 ([GFP-KlpA*Ncd-#2] = 2.5 nM) mainly exhibited
151 diffusive motion on the microtubules with no directional preference for either end (Fig. 2d;
152 Supplementary Movie 10). However, in motility experiments with 2.5 nM GFP-KlpA*Ncd-#2 and
153 80 nM TinA-mCherry, GFP-KlpA*Ncd-#2 and TinA-mCherry were observed to co-translocate
154 continuously on the microtubules toward the minus ends (Fig. 2e; Supplementary Movie 11).

155 Collectively, these results suggest that TinA mainly binds to the central stalk (a.a 100-398) of KlpA
156 to form the minus-end-directed KlpA-TinA complexes.

157 **The C-terminus of TinA plays a dual-functional role in KlpA-TinA complexes.** In the control
158 motility experiments, TinA was observed to bind to microtubules (Supplementary Fig. 1c, middle
159 panel), indicating that TinA functions as a microtubule-binding protein. Microtubule-associated
160 proteins often contain clusters of basic residues within their microtubule-binding regions[24–28].
161 Consistent with this, we found that the C-terminal region of TinA (a.a. 370–553) contains an
162 abundance of basic residues (Fig. 3a). To validate whether TinA is a microtubule-binding protein
163 and assess the contribution of its C-terminal region, we generated TinAΔC1-mCherry (Fig. 3b),
164 which lacks the C-terminal a.a. 370–553. We then performed in vitro microtubule co-
165 sedimentation experiments with both TinA-mCherry and TinAΔC1-mCherry. Our results showed
166 that TinA-mCherry co-precipitated with microtubules (Fig. 3c, left panel), whereas TinAΔC1-
167 mCherry retained the ability to bind to the microtubules, albeit with a reduced affinity compared
168 to TinA-mCherry (Fig. 3c, right panel). These findings indicate that the C-terminus of TinA
169 constitutes, or at least contributes to, a microtubule-binding motif**.**

170 To investigate whether the C-terminal region of TinA (a.a. 370–553) influences the motility
171 of KlpA-TinA complexes, we conducted motility experiments with 2.5 nM GFP-KlpA and varying
172 concentrations of TinAΔC1-mCherry. At 4 nM TinAΔC1-mCherry, the motility of GFP-KlpA was
173 largely unaffected, with GFP-KlpA only occasionally observed co-translocating with TinAΔC1-
174 mCherry toward microtubule minus ends (Fig. 3d, Supplementary Movie 12). However, at 80 nM
175 TinAΔC1-mCherry, more TinAΔC1-mCherry molecules were observed to co-translocate with
176 GFP-KlpA toward the microtubule minus end (Fig. 3e and Supplementary Movie 13). Collectively,
177 these motility results suggest that without the C-terminus, the ability of TinA to interact with KlpA
178 to form minus-end-directed complexes is severely impaired but not abolished entirely.
179 Interestingly, KlpA-TinAΔC1 complexes exhibited a single velocity mode comparable to the fast

180 mode of the KlpA-TinA complexes (V_{fast} = 321 ± 82, mean ± s.d., n = 244, Fig. 3f). This finding
181 implies that the C-terminus of TinA is responsible for the slow velocity mode observed in minus-
182 end-directed KlpA-TinA complexes (Fig. 1d,e).

183 **DISCUSSION**

184 To summarize, we investigated the effect of TinA on the motility of KlpA, a kinesin14 motor that
185 uniquely exhibits plus-end-directed motility on single microtubules as individual homodimers. We
186 revealed that TinA directly interacts with KlpA, enabling the kinesin-14 motor to reverse its
187 directionality and exhibit continuous motility towards the microtubule minus ends. To our
188 knowledge, TinA is the first protein that has been demonstrated capable of inducing directional
189 reversal in any kinesin through direct interaction. This finding markedly expands current
190 understanding of the scope of kinesin regulation by binding partners.

191 How does TinA enable KlpA to reverse directionality? We previously showed that KlpA
192 reverses its directionality in two scenarios: either when its N-terminal tail detaches from the
193 microtubule to which its motor domains bind[19], or when its N-terminal tail and C-terminal motor
194 domains are mechanically decoupled via the insertion of a flexible peptide in the central stalk[23].
195 Given that TinA binds directly to the central stalk of KlpA (Fig. 2), we suggest that TinA binding
196 alters the structure of the central stalk of KlpA. This alteration may either decouple the N-terminal
197 tail and C-terminal motor domains of KlpA or cause the N-terminal tail of KlpA to detach from the
198 microtubule, thus enabling the kinesin-14 motor to change its directionality. The precise
199 mechanism underlying this process awaits elucidation through future structural studies.

200 In addition to activating KlpA for minus-end directionality, TinA also enables KlpA to exhibit
201 processive motility on the microtubules (Fig. 1d,e). Our results showed that in the GFP channel,
202 minus-end-directed KlpA-TinA complexes are noticeably brighter than those individual GFP-KlpA
203 homodimers moving in the opposite direction (Fig. 1d), indicating that TinA recruits two or more
204 KlpA molecules to form individual minus-end-directed complexes. Having two or more KlpA
205 molecules is sufficient for these minus-end-directed KlpA-TinA complexes to achieve processive

206 motility on the microtubules, as clustering of as few as two or more nonprocessive kinesin-14
207 motors has been demonstrated to yield highly processive minus-end-directed motility[29,30].
208 We serendipitously discovered that TinA is a microtubule-binding protein (Fig. 3c). The C-
209 terminus of TinA (a.a. 370-553) constitutes, or at least contributes to, a microtubule-binding motif,
210 as removal of the C-terminal region weakens but does not abolish entirely the ability of TinA to
211 bind to the microtubules (Fig. 3b). In principle, TinA can use its C-terminus to enhance the
212 processivity of the resultant KlpA-TinA complexes, as studies have shown that several kinesins
213 gain processive motility via nonmotor microtubule-binding sites[14,17]. Surprisingly, we found that
214 TinA∆C1-mCherry (which lacks the C-terminal a.a. 370-553 and shows reduced microtubule
215 binding) appears to have lost the ability to interact with GFP-KlpA to form minus-end-directed
216 complexes in the motility experiments with 2.5 nM GFP-KlpA and 4 nM TinA∆C1-mCherry (Fig.
217 3d); but the formation of the minus-end-directed complexes can be partially rescued by increasing
218 the concentration of TinA∆C1-mCherry in the motility experiments (Fig. 3e). Thus, the C-terminus
219 of TinA contributes to enhancing the formation of the KlpA-TinA complexes, but is not involved in
220 the binding interface between TinA and KlpA. How does the C-terminus of TinA contribute to the
221 formation of the KlpA-TinA complexes without directly participating in the binding interface? We
222 suggest that the formation of the KlpA-TinA complexes occurs primarily on the microtubule lattice
223 rather than in the solution (Fig. 4). In this model, the C-terminus of TinA (a.a. 370-553) acts as a
224 primary microtubule-binding tether, which allows TinA to encounter and interact with multiple KlpA
225 molecules on the microtubule lattice to form the KlpA-TinA complexes (Fig. 4a). Without the C-
226 terminal a.a. 370-553, TinA∆C1 is unable to bind to the microtubule as strongly as the wildtype
227 TinA (Fig. 3c, right panel). Consequently, the chance of TinA∆C1 to encounter and interact with
228 multiple KlpA molecules on the microtubule lattice for forming the minus-end-directed complexes
229 is significantly impaired (Fig. 3d,e). Consistent with this model, we found that while KlpA-TinA
230 complexes were readily observed on the microtubules in the motility experiments (Fig. 1d,e), the
231 complexes were not observable in the absence of the microtubules using the standard

232 biochemical methods such as gel filtration and sucrose density gradient centrifugation (data not
233 shown). We further suggest that once KlpA-TinA complexes are formed on the microtubule, the
234 C-terminus of TinA in the complexes can either stay attached to or detached from the microtubule
235 (Fig. 4b). When the C-terminus of TinA in a KlpA-TinA complex is attached to the microtubule
236 (Fig. 4b, top panel), the complex exhibits slow minus-end-directed motility (Fig. 1d); and when the
237 C-terminus of TinA detaches from the microtubule (Fig. 4b, bottom panel), the KlpA-TinA complex
238 exhibits fast minus-end-directed motility (Fig. 3e).

239 Our study provides critical mechanistic insights into how TinA enables KlpA to exhibit
240 continuous minus-end-directed motility on microtubules. However, several important questions
241 remain unanswered. One key question pertains to the binding interface of the KlpA-TinA complex.
242 Due to the lack of high-resolution structural data for KlpA, TinA, or the KlpA-TinA complex, we
243 were unable to determine the precise binding interface in this study. Another question involves
244 the role of AnWdr8. In S. pombe, the localization of Pkl1 (a KlpA homolog) to the spindle poles
245 requires both Msd1 (a TinA homolog) and Wdr8[20] . Interestingly, our findings show that TinA alone
246 is sufficient to enable KlpA to exhibit continuous minus-end-directed motility. This observation
247 raises the intriguing possibility that in *A. nidulans*, AnWdr8 may not actively participate in KlpA
248 localization to the spindle poles but instead primarily functions to anchor the kinesin-14 motor at
249 these sites. Additionally, we note that the C-terminus of TinA, while absent in Msd1 from S. pombe,
250 is highly conserved among TinA-like proteins in fungi (Supplementary Fig. 2). This divergence
251 raises important questions about the extent to which the regulatory mechanisms of KlpA and Pkl1
252 are conserved. Addressing these questions will further enhance our understanding of the
253 regulatory mechanisms governing kinesin-14s during mitotic spindle assembly.

254 **ACKNOWLEDGEMENTS**

255 This work was supported by the National Institutes of Health (GM127922 to W.Q.).

256 **AUTHOR CONTRIBUTIONS**

257 W.Q. conceived, designed and supervised the project; A.V. designed and conducted all

experiments and performed the analysis; A.R.P. designed and conducted the initial experiments; Y.G. performed the analysis; all authors participated in interpreting the results; and W.Q. wrote the manuscript with the input from other authors.

COMPETING FINANCIAL INTERESTS

The authors declare no competing financial interests.

FIGURE LEGENDS

Figure 1: TinA enables KlpA to exhibit minus-end-directed motility with two distinct velocity modes. (**a**) Schematic diagrams of GFP-KlpA and TinA-mCherry. (**b**) The schematic diagram of the in vitro motility assay. (**c**) A representative kymograph showing that in the absence of TinA-mCherry, GFP-KlpA molecules exhibited plus-end-directed motility on a single microtubule. The white arrowhead indicates a GFP-KlpA aggregate moving toward the microtubule minus end. The motility experiment was performed with 2.5 nM GFP-KlpA in the motility chamber. Horizontal scale bar, 10 μm; vertical scale bar, 1 minute. (**d**) Representative kymographs showing that in the presence of a relatively high concentration of TinA-mCherry, GFP-KlpA molecules all exhibited minus-end-directed motility on a single microtubule and co-translocated toward the minus end with TinA-mCherry. The motility experiment was performed with 2.5 nM GFP-KlpA and 80 nM TinA-mCherry in the motility chamber. Horizontal scale bar, 10 μm; vertical scale bar, 1 minute. White arrowheads indicate kymograph segments with fast minus-end-directed motility, and blue arrowhead indicate kymograph segments with slow minus-end-directed motility. (**e**) Representative kymographs showing that in the presence of a much lower concentration of TinA-mCherry, a small number of GFP-KlpA molecules became minus-end-directed and co-translocated with TinA-mCherry toward the minus end on a single microtubule. The motility experiment was performed with 2.5 nM GFP-KlpA and 4 nM TinA-mCherry in the motility chamber. Horizontal scale bar, 10 μm; vertical scale bar, 1 minute. (**f**) The velocity histogram of minus-end-directed KlpA-TinA complexes. The histogram was generated from motility experiments with 2.5 nM GFP-KlpA and 4 nM TinA∆C1-mCherry. The velocity histogram

284 was fitted to a bimodal distribution, as indicated by the red curve. The green and blue curves
285 indicate the slow and fast distributions, respectively.

286 **Figure 2: TinA binds to the central stalk of KlpA.** (**a**) Schematic diagrams of GFP-KlpA, GFP-
287 KlpA*Ncd-#1, GFP-KlpA*Ncd-#2, and GFP-Ncd. (**b**) A representative kymograph showing that
288 GFP-KlpA*Ncd-#1 exhibited diffusive motion with no directionality preference on a single
289 microtubule. Horizontal scale bar, 10 μm; vertical scale bar, 1 minute. The motility experiment
290 was performed with 2.5 nM GFP-KlpA*Ncd-#1 in the motility chamber. (**c**) Representative
291 kymographs showing that in the presence of a relatively high concentration of TinA-mCherry,
292 GFP-KlpA*Ncd-#1 exhibited minus-end-directed motility and co-translocated with TinA-mCherry.
293 The motility experiment was performed with 2.5 nM GFP-KlpA*Ncd-#1 and 80 nM TinA-mCherry
294 in the motility chamber. Horizontal scale bar, 10 μm; vertical scale bar, 1 minute. (**d**) A
295 representative kymograph showing that GFP-KlpA*Ncd#2 exhibited diffusive motility with no
296 directional preference on a single microtubule. Horizontal scale bar, 10 μm; vertical scale bar, 1
297 minute. The motility experiment was performed with 2.5 nM GFP-KlpA*Ncd#2 in the motility
298 chamber. (**e**) Representative kymographs showing that in the presence of a relatively high
299 concentration of TinA-mCherry, GFP-KlpA*Ncd#2 exhibited minus-end-directed motility on a
300 single microtubule and co-translocated with TinA-mCherry toward the minus end. The motility
301 experiment was performed with 2.5 nM GFP-KlpA*Ncd#2 and 80 nM TinA-mCherry in the motility
302 chamber. Horizontal scale bar, 10 μm; vertical scale bar, 1 minute.

303 **Figure 3: The C-terminus of TinA affects the formation and velocity distribution of KlpA-**
304 **TinA complexes.** (**a**) The C-terminus of TinA (a.a. 370-553) contains an abundance of basic
305 residues. (**b**) Schematic diagrams of TinA and TinAΔC1-mCherry. (**c**) Coomassie-stained SDS-
306 PAGE gels from the microtubule co-sedimentation experiments for TinA-mCherry (Left Panel)
307 and TinAΔC1-mCherry (Right Panel). (**d**) Representative kymographs showing that minus-end-
308 directed KlpA-TinAΔC1 complexes were very rarely observed when the motility experiments were
309 performed with 2.5 nM GFP-KlpA and 4 nM TinAΔC1-mCherry. Horizontal scale bar, 10 μm;

310 vertical scale bar, 1 minute. (**e**) Representative kymographs showing that many more minus-end-
311 directed KlpA-TinAΔC1 complexes were observed when the motility experiments were performed
312 with 2.5 nM GFP-KlpA and 80 nM TinAΔC1-mCherry. Horizontal scale bar, 10 μm; vertical scale
313 bar, 1 minute. (**f**) The velocity histogram of minus-end-directed KlpA-TinAΔC1 complexes. The
314 histogram was generated from motility experiments with 2.5 nM GFP-KlpA and 80 nM TinAΔC1-
315 mCherry. The histogram was fitted to a single Gaussian distribution, as indicated by the blue
316 curve.

317 **Figure 4: A schematic model for the formation and motility of KlpA-TinA complexes.** (**a**)
318 TinA and KlpA interact to form the KlpA-TinA complexes on the microtubule lattice. Prior to
319 interacting with each other to form the KlpA-TinA complexes, KlpA exhibits plus-end-directed
320 motility by binding its N-terminal tail and C-terminal motor domains to the same microtubule, while
321 TinA binds to the microtubule lattice primarily through its C-terminus (a.a. 370-553). (**b**) TinA binds
322 to the central stalk of KlpA to enable the kinesin-14 motor to exhibit minus-end-directed motility
323 with two different velocity modes. The velocity modes of the KlpA-TinA complexes depends on
324 the microtubule-binding state of the C-terminus of TinA. KlpA-TinA complexes exhibit slow minus-
325 end-directed motility when the C-terminus of TinA binds to the microtubule lattice (top panel), but
326 switch to exhibit fast minus-end-directed motility when the C-terminus of TinA detaches from the
327 microtubule lattice (bottom panel).

328 **METHODS**

329 **Molecular cloning of recombinant KlpA constructs.** cDNAs of KlpA, Ncd and TinA were
330 codon-optimized and synthesized (IDT) for enhanced protein expression in bacteria. All
331 recombinant KlpA, Ncd and TinA constructs were integrated into a modified pET-17b vector
332 (Novagen) using either the Gibson assembly cloning kit (NEB) or the Q5 site-directed
333 mutagenesis kit (NEB) and verified by DNA sequencing (Azenta). All protein constructs contained
334 a 6xHis tag (at the N-terminus for all kinesin-14 constructs and at the C-terminus for all TinA
335 constructs) for protein purification. Additionally, all kinesin-14 constructs contained a GFP tag

336 after the N-terminal 6xHis tag, and all TinA constructs contained a mCherry tag before the C-
337 terminal 6xHis tag.

338 **Protein expression and purification.** All protein constructs were expressed in BL21(DE3)
339 Rosetta cells (Novagen). Cells were grown at 37 °C in tryptone phosphate medium (TPM)
340 supplemented with 50 mg/ml Ampicillin until OD600 reached 0.6-0.8. Expression was induced
341 with 0.1 mM isopropyl-b-D-thiogalactoside for 12–14 h at 18 °C. Cells were then harvested by
342 centrifugation, flash-frozen in liquid nitrogen, and stored at -80 °C.

343 For protein purification, cell pellets were resuspended in 50 mM sodium phosphate (NaPi)
344 buffer (pH 7.2) containing 250 mM NaCl, 1 mM $MgCl_2$, 0.5 mM ATP, 10 mM b-mercaptoethanol,
345 5% glycerol, and 20 mM imidazole in the presence of a protease inhibitor cocktail
346 (phenylmethylsulfonyl fluoride, leupeptin, and pepstatin) and then lysed via sonication. After
347 centrifugation at 27200 *g* for 30 min, soluble protein in the supernatant was purified by Talon resin
348 (Clontech) and eluted into 50 mM NaPi buffer (pH 7.2) containing 250 mM NaCl, 1 mM $MgCl_2$,
349 0.5 mM ATP, 10 mM b-mercaptoethanol, 5% glycerol and 250 mM imidazole. Protein was then
350 flash-frozen in liquid nitrogen and stored at -80 °C. For TinA proteins, ATP was excluded from the
351 purification buffers.

352 **Preparation of polarity-marked microtubules.** Unlabeled tubulin was purified from the porcine
353 brain via the assembly and disassembly method. Polarity-marked microtubules (HiLyte 647) with
354 bright plus ends were prepared as previously described[31]. Briefly, a tubulin mix (containing 1.7
355 mg/mL unlabeled tubulin and 1.2 mg/mL biotin-labeled tubulin) was first incubated in BRB80 (80
356 mM PIPES, pH 6.8, 1 mM EGTA, and 1 mM $MgCl_2$) with 0.125 mM guanosine-5'-[(a,b)-
357 methyleno]triphosphate (GMPCPP, Jena Bioscience) at 37 °C for 8-10 hours to allow tubulin to
358 polymerize to form microtubules. The resulting tubulin/microtubule mix was then centrifuged using
359 a TLA100 rotor (Beckman) at 279,000 *g* for 7 minutes at 37 °C. To cap the microtubule plus ends,
360 the pellet was resuspended in a bright tubulin mix, which contains 0.75 mg/mL unlabeled tubulin,
361 0.14 mg/mL HiLyte Fluor647-labeled tubulin (Cytoskeleton) and 1.5 mg/mL N-ethylmaleimide-

362 tubulin in BRB80 with 0.1 mM GMPCPP, and further incubated at 37 °C for additional 45 minutes.
363 The resulting polarity-marked microtubules were first pelleted using a TLA100 rotor at 9800 *g* for
364 7 minutes at 37 °C and then resuspended in BRB80 with 40 μM Taxol.

365 **Total internal reflection fluorescence (TIRF) microscopy.** All time-lapse imaging experiments
366 were performed at room temperature using the Axio Observer Z1 objective-type TIRF microscope
367 (Zeiss) equipped with a 100x, 1.46 numerical aperture oil-immersion objective and a back-thinned
368 electron multiplier charge-coupled device camera (Photometrics). All experiments used
369 microscope coverslips that were functionalized with biotinylated polyethylene glycol (biotin-PEG)
370 as previously described to reduce nonspecific surface absorption of molecules[32]. All time-lapse
371 imaging experiments in this study used flow cells that were made by attaching a coverslip to a
372 microscope glass slide by double-sided tape.

373 **In vitro motility assays.** For all in vitro motility experiments, the motility chamber was perfused
374 with 0.5 mg/ml streptavidin for immobilizing polarity-marked HyLite 647 microtubules. The
375 chamber was washed twice to remove an unbound streptavidin with buffer A (BRB12
376 supplemented with 20 μM taxol). The polarity-marked HyLite 647 microtubules were then added
377 and immobilized on the functionalized coverslip for 5 minutes. Unbound microtubules were
378 washed out from the chamber twice with buffer B (BRB50 supplemented with 1.3 mg/ml casein
379 and 20 μM taxol). For the motility experiments of GFP-tagged kinesin-14 molecules (GFP-KlpA,
380 GFP-KlpAΔN^T, GFP-KlpA*Ncd-#1, GFP-KlpA*Ncd-#2, and GFP-Ncd) in the presence of
381 mCherry-labeled TinA variants (TinA-mCherry and TinAΔC1-mCherry), GFP-tagged kinesin-14
382 and mCherry-labeled TinA variants were diluted in buffer B and mixed in the motility buffer C
383 (BRB50 supplemented with 25 mM KCl, 1 mM ATP, 25 μM taxol, 1.3 mg/ml casein, and an oxygen
384 scavenger system) for a final concentration of 2.5 nM and either 4 nM or 80 nM, respectively,
385 before added to the chamber. The images were taken immediately after focusing. Time-lapse
386 images were acquired for a total duration of 10 minutes at 1 frame per second with an exposure

387 time of 100 ms for all channels. Kymographs were generated and analyzed using Fiji[33] . The
388 velocity distributions were generated and analyzed in Python[34] .

389 **Microtubule co-sedimentation assays.** For all microtubule co-sedimentation experiments,
390 taxol-stabilized microtubules were prepared as previously described[35]. Briefly, unlabeled-tubulin
391 (20 μM) was incubated on ice for 3 minutes, mixed gently with polymerization buffer (BRB80
392 supplemented with 2 mM MgCl2, 2 mM GTP, 2 mM DTT, and 20% DMSO), and incubated on ice
393 for additional 3 minutes. The mixture was then incubated at 37 °C for 30 minutes. Polymerized
394 microtubules were mixed with microtubule-stabilizing buffer (BRB80 supplemented with 1 mM
395 DTT and 40 μM taxol) and incubated at 37 °C for additional 30 minutes. Purified TinA-mCherry
396 and TinAΔC1-mCherry were each mixed with taxol-stabilized microtubules in BRB50
397 supplemented with 25 mM KCl, 1.3 mg/mL casein, 1% ß-mercaptoethanol, and 40 μM taxol. The
398 mixture was incubated at room temperature for 30 minutes and centrifuged at 100000 *g* using a
399 TLA100 rotor for 20 minutes at 25 °C. Coomassie-stained SDS-PAGE gels were used for
400 comparing the amount of protein in the supernatant and pellet fractions.

401

402 **REFERENCE**

403 1. Pavin, N. & Tolić, I. M. Mechanobiology of the Mitotic Spindle. *Dev. Cell* **56**, 192–201 (2021).

404 2. Gudimchuk, N. B. & McIntosh, J. R. Regulation of microtubule dynamics, mechanics and
405 function through the growing tip. *Nat. Rev. Mol. Cell Bio.* **22**, 777–795 (2021).

406 3. Wordeman, L. How kinesin motor proteins drive mitotic spindle function: Lessons from
407 molecular assays. *Semin. Cell Dev. Biol.* **21**, 260–268 (2010).

408 4. Winey, M. & Bloom, K. Mitotic Spindle Form and Function. *Genetics* **190**, 1197–1224 (2012).

409 5. Hirokawa, N., Noda, Y., Tanaka, Y. & Niwa, S. Kinesin superfamily motor proteins and
410 intracellular transport. *Nat. Rev. Mol. Cell Bio.* **10**, 682–696 (2009).

411 6. Sansregret, L. & Swanton, C. The Role of Aneuploidy in Cancer Evolution. *Cold Spring Harb.*
412 *Perspect. Med.* **7**, a028373 (2017).

413 7. Lawrence, C. J. *et al.* A standardized kinesin nomenclature. *J. Cell Biol.* **167**, 19–22 (2004).

414 8. She, Z.-Y. & Yang, W.-X. Molecular mechanisms of kinesin-14 motors in spindle assembly and
415 chromosome segregation. *J Cell Sci.* **130**, 2097–2110 (2017).

416 9. Norris, S. R. *et al.* Microtubule minus-end aster organization is driven by processive HSET-
417 tubulin clusters. *Nat. Commun.* **9**, 2659 (2018).

418 10. Walker, R. A., Salmon, E. D. & Endow, S. A. The Drosophila claret segregation protein is a
419 minus-end directed motor molecule. *Nature* **347**, 780–782 (1990).

420 11. McDonald, H. B. & Goldstein, L. S. B. Identification and characterization of a gene encoding
421 a kinesin-like protein in Drosophila. *Cell* **61**, 991–1000 (1990).

422 12. Furuta, K., Edamatsu, M., Maeda, Y. & Toyoshima, Y. Y. Diffusion and directed movement:
423 In vitro motile properties of fission yeast kinesin-14 Pkl1. *J. Biol. Chem.* **283**, 36465–36473 (2008).

424 13. O'Connell, M. J., Meluh, P. B., Rose, M. D. & Morris, N. R. Suppression of the bimC4 mitotic
425 spindle defect by deletion of klpA, a gene encoding a KAR3-related kinesin-like protein in
426 Aspergillus nidulans. *J. Cell Biol.* **120**, 153–162 (1993).

427 14. Mieck, C. *et al.* Non-catalytic motor domains enable processive movement and functional
428 diversification of the kinesin-14 Kar3. *Elife* **4**, e04489 (2015).

429 15. Tseng, K.-F. *et al.* The Tail of Kinesin-14a in Giardia Is a Dual Regulator of Motility. *Curr. Biol.*
430 **30**, 3664-3671.e4 (2020).

431 16. Reinemann, D. N., Norris, S. R., Ohi, R. & Lang, M. J. Processive Kinesin-14 HSET Exhibits
432 Directional Flexibility Depending on Motor Traffic. *Curr. Biol.* **28**, 2356-2362.e5 (2018).

433 17. Tseng, K.-F. *et al.* The preprophase band-associated kinesin-14 OsKCH2 is a processive
434 minus-end-directed microtubule motor. *Nat. Commun.* **9**, 1067 (2018).

435 18. Walter, W. J., Machens, I., Rafieian, F. & Diez, S. The non-processive rice kinesin-14 OsKCH1
436 transports actin filaments along microtubules with two distinct velocities. *Nat. Plants* **1**, 15111
437 (2015).

438 19. Popchock, A. R. *et al.* The mitotic kinesin-14 KlpA contains a context-dependent directionality
439 switch. *Nat. Commun.* **8**, 13999 (2017).

440 20. Yukawa, M., Ikebe, C. & Toda, T. The Msd1–Wdr8–Pkl1 complex anchors microtubule minus
441 ends to fission yeast spindle pole bodies. *J. Cell Biol.* **209**, 549–562 (2015).

442 21. Hori, A. *et al.* The conserved Wdr8-hMsd1/SSX2IP complex localises to the centrosome and
443 ensures proper spindle length and orientation. *Biochem. Bioph. Res.* **468**, 39–45 (2015).

444 22. Shen, K.-F. & Osmani, S. A. Regulation of mitosis by the NIMA kinase involves TINA and its
445 newly discovered partner, An-WDR8, at spindle pole bodies. *Mol. Biol. Cell* **24**, 3842–3856 (2013).

446 23. Wang, P. *et al.* The Central Stalk Determines the Motility of Mitotic Kinesin-14 Homodimers.
447 *Curr. Biol.* **28**, 2302-2308.e3 (2018).

24. Aizawa, H. *et al.* Molecular cloning of a ubiquitously distributed microtubule-associated protein with Mr 190,000. *J. Biol. Chem.* **265**, 13849–13855 (1990).

25. Lee, G., Cowan, N. & Kirschner, M. The Primary Structure and Heterogeneity of Tau Protein from Mouse Brain. *Science* **239**, 285–288 (1988).

26. Lewis, S. A., Wang, D. H. & Cowan, N. J. Microtubule-Associated Protein MAP2 Shares a Microtubule Binding Motif with Tau Protein. *Science* **242**, 936–939 (1988).

27. Noble, M., Lewis, S. A. & Cowan, N. J. The microtubule binding domain of microtubule-associated protein MAP1B contains a repeated sequence motif unrelated to that of MAP2 and tau. *J. Cell Biol.* **109**, 3367–3376 (1989).

28. Ludzia, P. *et al.* Structural characterization of KKT4, an unconventional microtubule-binding kinetochore protein. *Structure* **29**, 1014-1028.e8 (2021).

29. Jonsson, E., Yamada, M., Vale, R. D. & Goshima, G. Clustering of a kinesin-14 motor enables processive retrograde microtubule-based transport in plants. *Na.t Plants* **1**, 15087 (2015).

30. Furuta, K. *et al.* Measuring collective transport by defined numbers of processive and nonprocessive kinesin motors. *Proc. Natl. Acad. Sci.* **110**, 501–506 (2013).

31. Hyman, A. A. Preparation of marked microtubules for the assay of the polarity of microtubule-based motors by fluorescence. *J. Cell Sci.* **1991**, 125–127 (1991).

32. Roberts, A. J., Goodman, B. S. & Reck-Peterson, S. L. Reconstitution of dynein transport to the microtubule plus end by kinesin. *Elife* **3**, e02641 (2014).

33. Schindelin, J. *et al.* Fiji: an open-source platform for biological-image analysis. *Nat. Methods* **9**, 676–682 (2012).

34. Virtanen, P. *et al.* SciPy 1.0: fundamental algorithms for scientific computing in Python. *Nat. Methods* **17**, 261–272 (2020).

35. Huang, T. G., Suhan, J. & Hackney, D. D. Drosophila kinesin motor domain extending to amino acid position 392 is dimeric when expressed in Escherichia coli. *J. Biol. Chem.* **269**, 16502–16507 (1994).

Figure 1

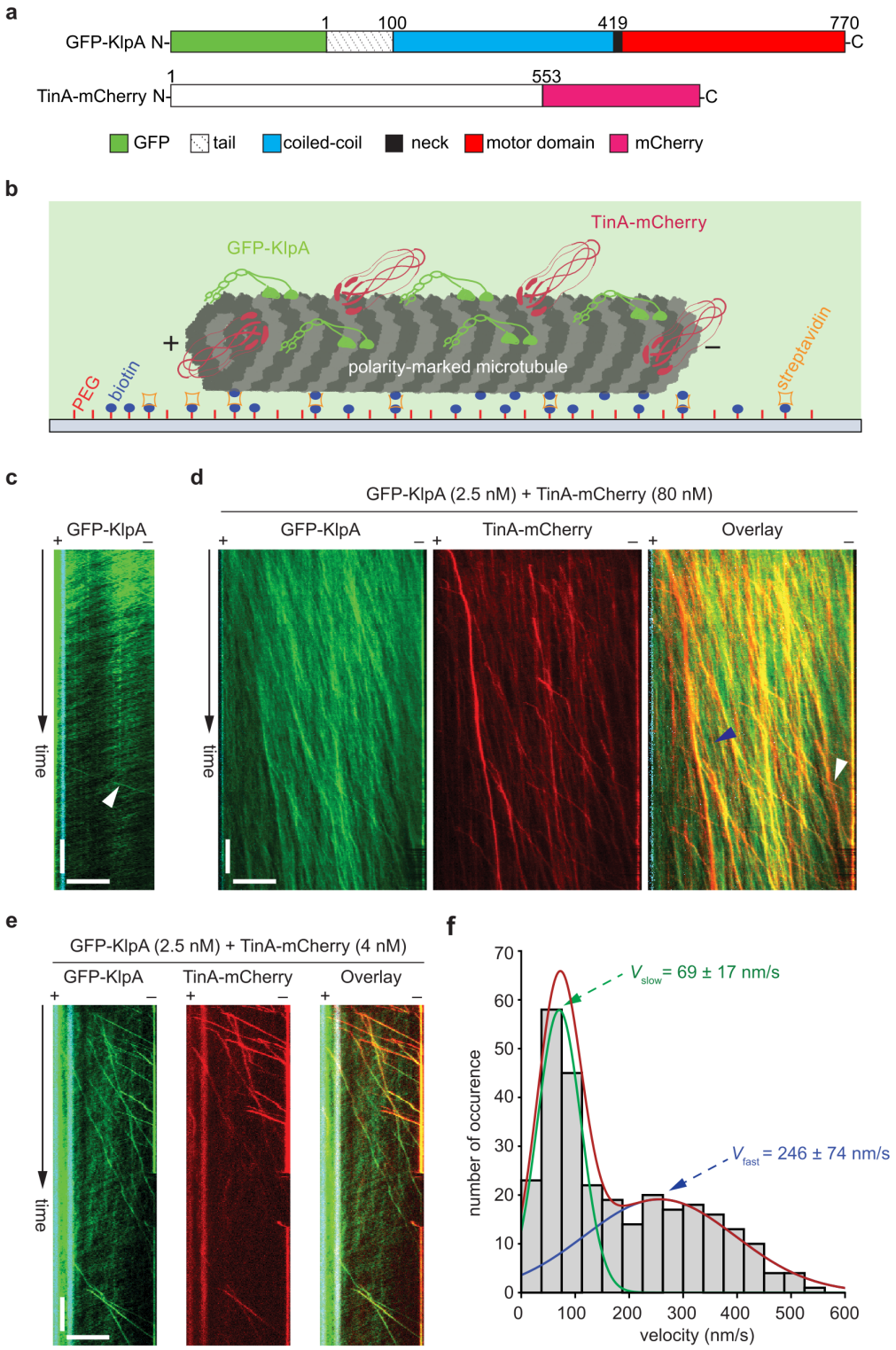
a
GFP-KlpA N-
1
100
419
770
-C
TinA-mCherry N-
1
553
-C
GFP
tail
coiled-coil
neck
motor domain
mCherry
b
TinA-mCherry
GFP-KlpA
+
–
polarity-marked microtubule
PEG
biotin
streptavidin
c
GFP-KlpA
+
–
time
d
GFP-KlpA (2.5 nM) + TinA-mCherry (80 nM)
GFP-KlpA
TinA-mCherry
Overlay
time
e
GFP-KlpA (2.5 nM) + TinA-mCherry (4 nM)
GFP-KlpA
TinA-mCherry
Overlay
time
f
V_{slow} = 69 ± 17 nm/s
V_{fast} = 246 ± 74 nm/s
number of occurence
velocity (nm/s)
0
10
20
30
40
50
60
70
0
100
200
300
400
500
600

Figure 2

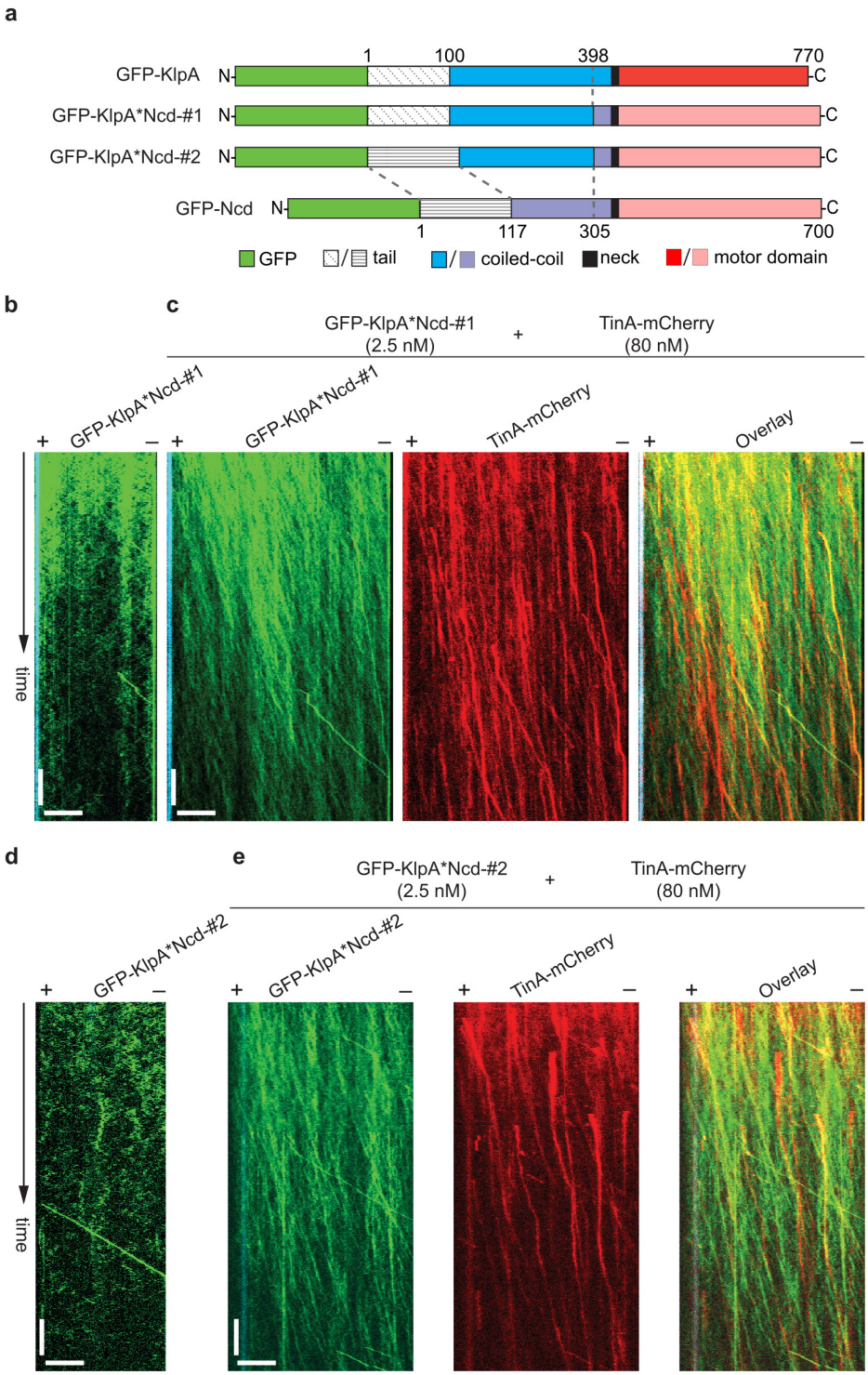
a
GFP-KlpA
GFP-KlpA*Ncd-#1
GFP-KlpA*Ncd-#2
GFP-Ncd
N-
-C
1
100
398
770
117
305
700
GFP
tail
coiled-coil
neck
motor domain
b
c
GFP-KlpA*Ncd-#1
(2.5 nM)
+
TinA-mCherry
(80 nM)
GFP-KlpA*Ncd-#1
TinA-mCherry
Overlay
time
d
e
GFP-KlpA*Ncd-#2
(2.5 nM)
TinA-mCherry
(80 nM)
GFP-KlpA*Ncd-#2
TinA-mCherry
Overlay

Figure 3

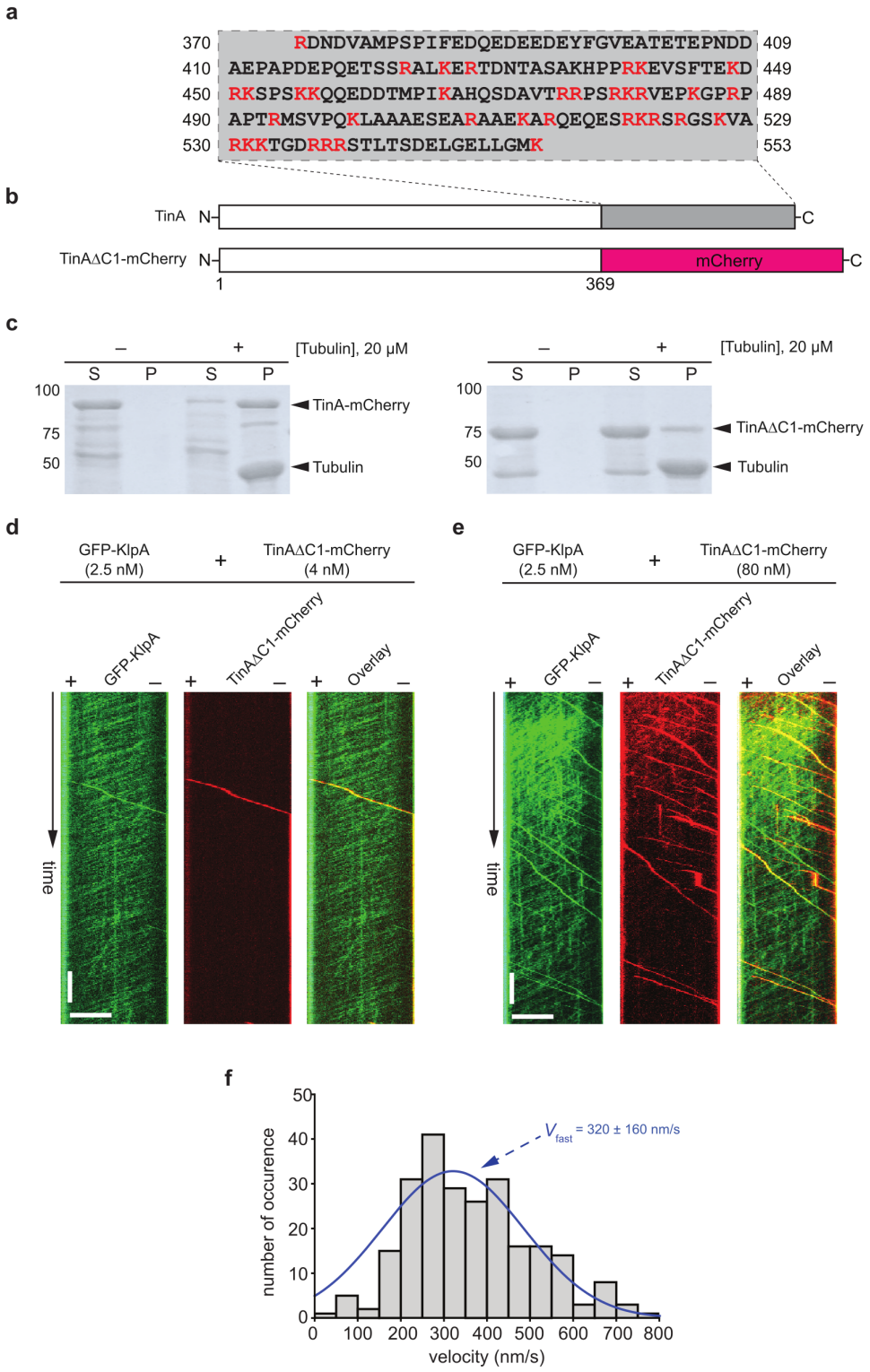
a
370 RDNDVAMPSPIFEDQEDEEDEYFGVEATETEPNDD 409
410 AEPAPDEPQETSSRALKERTDNTASAKHPPRKEVSFTEKD 449
450 RKSPSKKQQEDDTMPIKAHQSDAVTRRPSRKRVEPKGPRP 489
490 APTRMSVPQKLAAAESEARAAEKARQEQESRKRSRGSKVA 529
530 RKKTGDRRRSTLTSDELGELLGMK 553
b
TinA N C
TinAΔC1-mCherry N mCherry C
1
369
c
– + [Tubulin], 20 μM
S P S P
100
75
50
TinA-mCherry
Tubulin
TinAΔC1-mCherry
d
GFP-KlpA (2.5 nM) + TinAΔC1-mCherry (4 nM)
GFP-KlpA
TinAΔC1-mCherry
Overlay
time
e
GFP-KlpA (2.5 nM) + TinAΔC1-mCherry (80 nM)
f
number of occurence
velocity (nm/s)
V_{fast} = 320 ± 160 nm/s

Figure 4

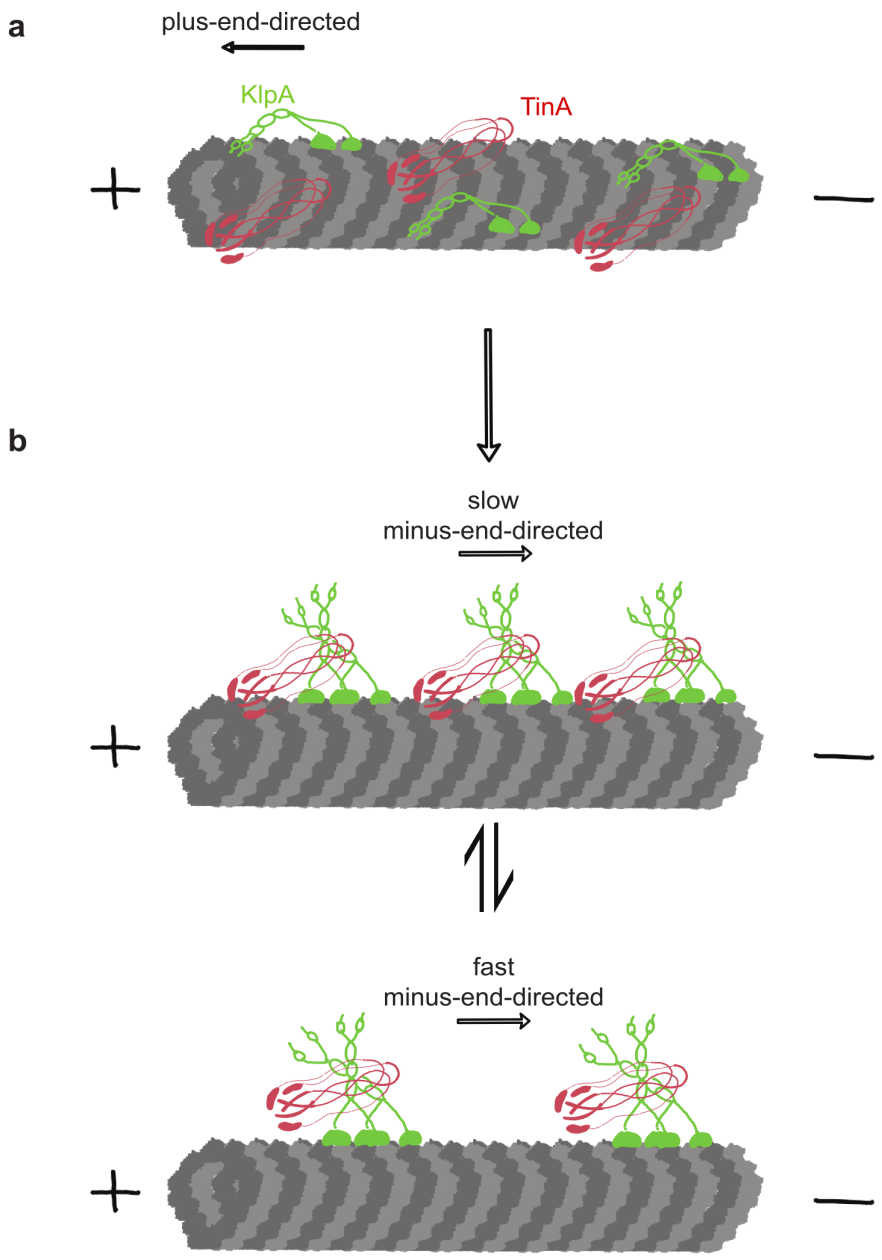
a
plus-end-directed
KlpA
TinA
+
−
b
slow
minus-end-directed
+
−
fast
minus-end-directed
+
−